Database of Petrophysical Properties of the Mid-German Crystalline High

Sebastian Weinert[1,2], Kristian Bär[1], Ingo Sass[1,2]

[1]Geothermal Science and Technology, Technical University of Darmstadt, Darmstadt, 64287, Germany
[2]Darmstadt Graduate School of Excellence Energy Science and Engineering, Technical University of Darmstadt, Darmstadt, 64287, Germany

Correspondence to: Sebastian Weinert (weinert@geo.tu-darmstadt.de)

Abstract. Petrophysical properties are a key element for reservoir characterization but also for interpreting the results of various geophysical exploration methods or geophysical well logs. Furthermore, petrophysical properties are commonly used to populate numerical models and are often critically governing the model results. Despite the common need of detailed petrophysical properties, data is still very scarce and often not available for the area of interest. Furthermore, both the online research for published property measurements or compilations, as well as dedicated measurements campaigns of the selected properties, which requires comprehensive laboratory equipment, can be very time-consuming and costly. To date, most published research results are often focused on a limited selection of parameters only and hence, researching various petrophysical properties, needed to account for the thermal-hydraulic-mechanical behavior of selected rock types or reservoir settings, can be very laborious.

Since for deep geothermal energy in central Europe, the majority of the geothermal potential or resource is assigned to the crystalline basement, a comprehensive database of petrophysical properties comprising rock densities, porosity, rock matrix permeability, thermal properties (thermal conductivity and diffusivity, specific heat capacity) as well as rock mechanical properties as compressional and shear wave velocities, unconfined compressive strength, Young's modulus, Poisson's ratio, tensile strength and triaxial shear strength was compiled by measurements conducted at the HydroThermikum lab facilities of the Technical University of Darmstadt.

Analyzed samples were mostly derived from abandoned or active quarries and natural or artificial outcrops such as road cuts, riverbanks, or steep hill slopes. Furthermore, samples of the cored deep wells Worms 3 (samples from 2175-2195 m), Stockstadt 33R (samples from 2245-2267 m), Weiterstadt 1 (samples from 2502-2504 m), Tiefbohrung Groß-Umstadt/Heubach, B/89 – B02 and the cored shallow wells Forschungsbohrung Messel GA 1 and 2 as well as GWM17 Zwingenberg, GWM1A Zwingenberg, Langenthal BK2/05, EWS267/1 Heubach, and archive samples of the Institut für Steinkonservierung e. V. in Mainz originating from a comprehensive large scale sampling campaign in 2007 were investigated.

The database (Weinert et al. 2020b, https://doi.org/10.25534/tudatalib-278) aims to provide easily accessible petrophysical properties of the Mid-German Crystalline High, measured on 224 locations in Bavaria, Hesse, Rhineland-Palatinate and

Thuringia and comprising 26,951 single data points. Each data point is addressed with the respective metadata such as sample identifier, sampling location, petrography and if applicable stratigraphy and sampling depth (in case of well samples).

1 Introduction

For geothermal energy, reservoir exploration often lacks dedicated slim-hole exploration wells to enhance the understanding of the physical and hydraulic behavior of the explored geothermal reservoir at an early project stage (Sass et al. 2016). Therefore, reservoir characterization often solely relies on either geophysical exploration or numerical models which, in turn, need petrophysical input parameters to be successful and accurate. Due to the sparseness of reservoir samples, explained by the high costs of coring deep wells, petrophysical properties can be derived from outcrop analogue studies (e.g. Howell et al., 2014 or Ukar et al., 2019) or literature data for suitable rock types (Bär et al., 2020). Nonetheless, even in rather isotropic, homogeneous material such as crystalline rocks, petrophysical properties can vary depending on their geochemical composition and texture (e.g. dataset of Krietsch et al., 2018 and references therein, Weinert et al., 2020a) but also physical appearance, micro-fractures or porosity (e.g. Mielke et al., 2017, Weinert et al., 2020a) as well as degree of alteration or weathering (e.g. Machek et al., 2013).

A profound understanding of the regarded rock type, its respective petrophysical properties and the methods how those were measured are essential for populating numerical simulations or interpreting geophysical exploration methods.

Despite the importance of petrophysical properties, as well as the importance of crystalline basement rocks in deep geothermal energy, to which 85% to 90% of the German geothermal potential is accredited (Deutscher Bundestag, 2003), such data is often either unpublished, only published for confined areas (e. g. Mielke et al., 2016, Aretz et al., 2016, Weydt et al., 2020, Weinert et al., 2020a) or published without important meta-information. The search for suitable petrophysical properties can therefore be very time-consuming and often, only widely averaged properties can be found and are commonly used neglecting local heterogeneities, vertical and lateral variability and anisotropic behavior of the rocks.

To overcome the lack of suitable petrophysical data, a sampling and measuring campaign was initiated within the scope of the Hessen 3D 2.0 project: '3D-Modell der petrothermalen und mitteltiefen Potenziale zur Wärmenutzung und -speicherung von Hessen' (Federal Ministry for Economic Affairs and Energy; funding number 0325944A) with the aim to develop a comprehensive database. This database of petrophysical properties of the Mid-German Crystalline High was supplemented and compiled to facilitate easy access to research data on measured petrophysical properties and to allow for an adequate generalization for specific petrological units within the Mid-German Crystalline High. Therefore, the database presented here (Weinert et al. 2020b, https://doi.org/10.25534/tudatalib-278) publicly provides all relevant laboratory measurements on the Mid-German Crystalline High samples of a variety of unpublished and published studies of the Technical University of Darmstadt as well as over 1,900 newly measured data points.

2 Mid-German Crystalline High

The Mid-German Crystalline High (MGCH) is a NE-SW striking Variscan complex of approx. 50-65 km width in NW-SE extension and several hundred kilometers length along strike. Locally exposed in the Pfälzer Wald, Odenwald, Spessart, Ruhla Mountains and Kyffhäuser Crystalline Complex, the MGCH is sandwiched between the Saxothuringian Zone to the SW and the Northern Phyllite Zone, which represents the southern suture zone of the Rhenohercynian belt to the NE (Fig. 1).

While the NW boundary between the MGCH and Northern Phyllite Zone is not exposed, the MGCH is fault-bounded to the Saxothuringian zone (Linnemann et al., 2008) to the SE.

The MGCH metamorphic and crystalline complexes are interpreted as the northern margin of Armorica (McCann et al., 2008) and hence a suture of the Rheic Ocean at the rim of the Bohemian Massif (Linnemann et al., 2008).

Outcrops of the MGCH display a variety of high-grade metamorphic Late Ordovician to Early Devonian rocks in the Böllsteiner Odenwald (450 Ma, Reischmann et al., 2001), the Spessart Crystalline Complex (418-407 Ma, Lippolt, 1986, Dombrowsky et al., 1995) or the Ruhla Crystalline Complex (413-400 Ma, Brätz, 2000, Zeh and Wunderlich, 2003). Mafic, intermediate and acid intrusive igneous rocks are preferentially exposed in the Bergsträsser Odenwald where they comprise up to 90% of the exposed rocks (Stein, 2001), as well as in the Spessart and Ruhla mountains. The northern part of the Odenwald (Frankenstein Complex) is predominantly comprised of Late Devonian gabbro (362±7 Ma, Kirsch et al., 1988) as well as metamorphic rocks. The southern part is composed of amphibolite-facies metamorphosed metasediments and gneiss (342-332 Ma, Todt et al., 1995) which were intruded by the undeformed Weschnitz, Tromm and Heidelberg plutons. Those intrusions are homogenous and comprised by monzodiorite to granodiorite (Weschnitz pluton), granite (Tromm pluton) and gabbro to diorite with later granite and granodiorite intrusions at the Heidelberg pluton (Timmerman, 2008). Post-tectonic carboniferous diorite and granodiorite dominate the SE part of the Spessart Crystalline complex (c. 330 Ma, Anthes and Reischmann, 2001) while Carboniferous granites predominantly occur in the Ruhla mountains (Timmerman, 2008).

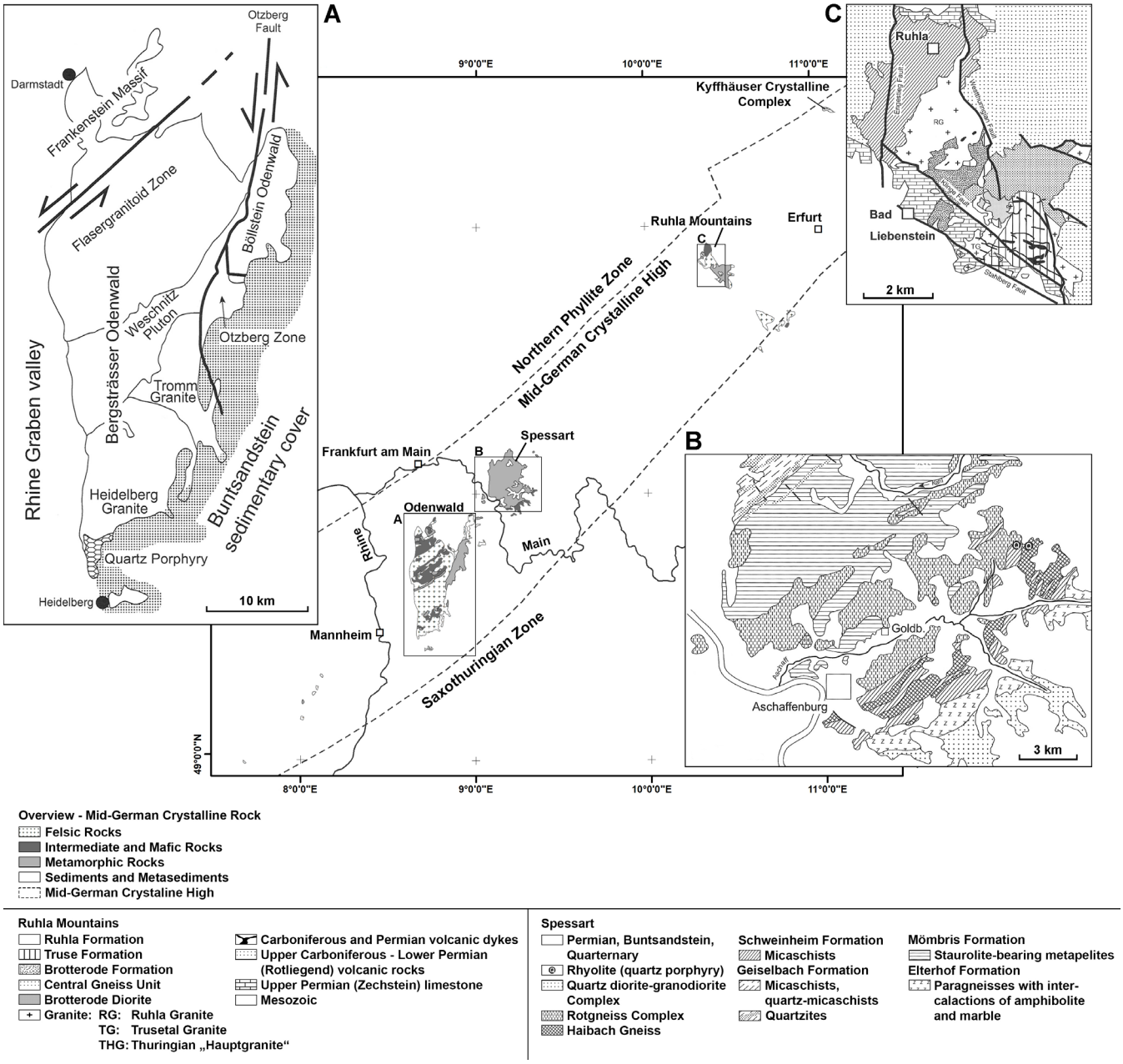

Figure 1: Simplified overview map after (Hirschmann 1995, Voges et al. 1993, Klügel 1997, Kroner et al. 2008) of the Mid-German Crystalline High outcrops (A) Odenwald (after Stein 2001; Will and Schmädicke 2001; McCann et al. 2008), (B) Spessart (after Okrusch 1983; Dombrowski et al. 1995; McCann et al. 2008) and (C) Ruhla Mountains (Zeh et al. 2003; McCann et al. 2008).

2 Contents and Structure of the Database

The database is provided in spreadsheet format as well as in delimited text file format. It is structured in two super-entities, namely 'metadata' and 'petrophysical properties' and further hierarchical structured into logical subdivisions.
While the metadata stores information about the sample location, sample ID but also stratigraphic and petrographic information, the actual measured petrophysical properties are summarized under petrophysical properties.
Each super-entity and its content are described in following sub-chapters in detail.

2.1 Metadata

The super-entity 'Metadata' comprises information concerning the sample identifier (sample ID) and its parent ID, the analyzer of the petrophysical properties, the sampling location but also stratigraphic and petrographic information and the sample dimensions if measured and documented.

2.1.1 Sample Information

The presented database renounces to unify sample IDs as other researches did (e.g. Bär et al., 2020) and instead only documents the original sample ID that was chosen by the analyzer. If multiple measurements were performed on a single sample (e.g. thermal conductivity on top and bottom end faces of cylindrical samples) the parental sample ID of the actual specimen is also provided. Therefore, reviewing original sources is feasible and allows to easily search for samples and further information such as detailed descriptions in the original sources. For all data extracted from either published or unpublished theses or reports, the referring reference is also given and indexed in the bibliography of both, the database (Weinert et al., 2020b) as well as the here presented work.
Although all the presented data were analyzed in the same institution applying the same laboratory equipment, the individual person analyzing the samples might affect the data during data gathering and result evaluation (for example picking shear wave velocities). While comparing datasets of different people slight variations can occur. Therefore, the person who has analyzed the samples is also stored in the sample information.

2.1.2 Sampling Location

Samples were taken from quarries, abandoned quarries, outcrops, wells (cored borehole sections) as well as the archive of the Institut für Steinkonservierung e. V. Knowledge of the sample origin is important in data evaluation. For example, samples taken in active quarries might be influenced due to excavation either by heavy machinery or explosives while samples from abandoned quarries and natural outcrops may be slightly to significantly weathered. Well samples were subdued to higher

temperature and pressure conditions and might show extension (micro-)fractures due to stress relief during core retrieval ('core-disking').

In addition to the outcrop type, information about the geographical origin of the sample are given by a location as well as the referring federal state and state of this location (e.g. location: E of Wingertsstraße, Alzenau; federal state: Hesse; country: Germany). Also, the location coordinates are indexed in the database and catalogued as decimal degree with the reference system WGS84. The elevation at the coordinate point is given in meters above mean sea level (MAMSL).

For well samples besides geographical information, also the well name and its respective archive number (if applicable) are indexed. The given elevation correlates with the well head elevation and the depth of the sample conforms to the measured depth (MD) below ground level (b.g.l.).

2.1.3 Stratigraphy

The stratigraphy documented in the database is divided into the period and series representing the sample. Additionally, a term for the formation or unit is given, which, if given, conforms with the locally used term.

According to international standards, the documented terms used for the stratigraphic period and series are corresponding to the international chronostratigraphic chart of the IUGS v2020/01 (Cohen et al., 2013, updated). For each stratigraphic period and series, a respective stratigraphic ID is provided which correlates with the stratigraphic IDs published in Bär et al. (2019a) and Bär et al. (2020).

2.1.4 Petrography

Petrographic metadata are given by a simplified petrographic term and a correlating petrographic ID and petrographic parent ID (Fig. 2). The petrographic IDs are corresponding to Bär et al. (2019b) which are based on the well database of Hessian Agency for Nature Conservation, Environment and Geology. Also based on the petrographic ID presented in Bär et al. (2019b) a parental petrographic ID for each sample is provided. Petrography is either evaluated microscopically on thin sections (if applicable) or macroscopically on fresh hand pieces.

2.1.5 Sample Dimensions

If measured, the sample height and diameter are reported in centimeter (cm). Additionally, the grain and bulk volume are documented in cubic centimeter (cm^{-3}) and sample weight is reported in grams (g).

2.2 Petrophysical Properties

The database presented here includes 20 kinds of petrophysical properties measured on a variety of samples. To increase readability, petrophysical properties are subdivided into thermophysical and rock mechanical properties (Table 1 and Table 2). All analysis performed on the same specimen are documented in the same row. For some methods such as thermal conductivity and diffusivity, multiple measurements at the identical sample are possible (e.g. top and bottom end face on the

145 sample). In case of multiple measurements, each single measurement is documented in a separate row (sample ID). Additionally, an average value and standard deviation is given for the specimen (parental sample ID).

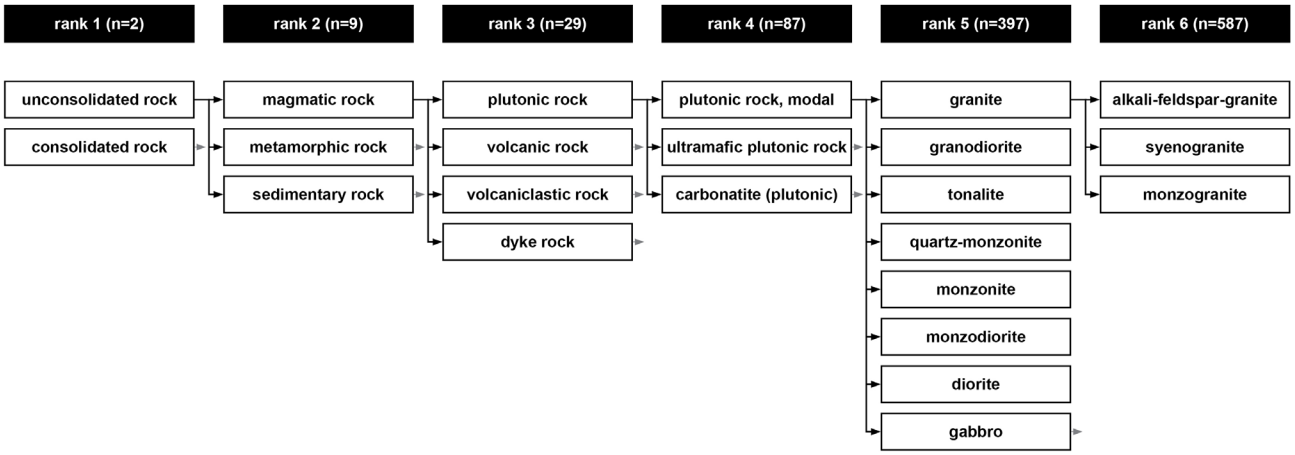

Figure 2: Hierarchical system of standardized petrographic terms referring to Bär et al. 2019b. Black boxes show the rank and 150 **number of entries within each rank, white boxes represent the specific term and show classification scheme on the example of granites. Black arrows indicate direct connections and grey arrows represent additional terms not displayed here.**

2.2.1 Thermophysical Properties

Documented thermophysical properties include grain and bulk density, porosity, thermal conductivity and diffusivity, specific heat capacity but also apparent and intrinsic permeability. Since thermal conductivity and thermal diffusivity is often measured 155 on multiple surfaces both parameters have three dedicated rows each. One row documents single measurements, one the average value of the sample and the last row documents the standard deviation of the average.

The total number of single thermophysical property measurements and average values are listed in Table 1.

Table 1: Number of measurements of thermophysical properties.

Property	Number of single measurements	Number of measured samples
Bulk density	974	974
Grain density	1,238	1,238
Porosity	918	918
Thermal conductivity	3,518	1,551
Thermal diffusivity	3,298	1,512
Specific heat capacity	1,415	1,415
Apparent and intrinsic permeability	991	991
Total	**12,353**	**8,600**

All measurements were conducted at the Technical University of Darmstadt and the applied methods are described in the following section.

2.2.2 Rock Mechanical Properties

Compressional and shear wave velocity, dynamic and static Young's modulus, dynamic and static Poisson's ratio, unconfined compressive strength, bulk modulus, tensile strength as well as triaxial shear strength, cohesion and angle of friction are summarized (Table 2). Compressional and shear wave velocities are often measured multiple times on the same specimen; therefore, each single measurement is listed as well as the respective sample average including the standard deviation. Since dynamic Young's modulus and Poisson's ratio are calculated using the compressive and shear strength, a sample average and standard deviation is also provided for them.

Table 2: Number of measurements of rock mechanical properties.

Property	Number of single measurements	Number of measured samples
Compressional wave velocity	1,247	822
Shear wave velocity	1,247	822
Dynamic Young's modulus	1,165	740
Dynamic Poisson's Ratio	1,247	822
Unconfined compressive strength	400	400
Static Young's modulus	185	185
Static Poisson's Ratio	180	180
Bulk modulus	116	116
Tensile Strength	231	231
Triaxial Shear Strength	106	106
Total	**5,816**	**4,116**

As for the petrophysical properties, all measurements were conducted at the Technical University of Darmstadt and the applied methods are described in the following section.

3 Methods

Measurements comprise grain density, bulk density, porosity, apparent and intrinsic permeability, thermal conductivity, thermal diffusivity, compressional and shear wave velocities as well as and at selected locations unconfined compressive

strength, Young's modulus, Poisson's ratio, tensile strength and triaxial shear strength including cohesion and coefficient of friction.

Prior to any measurement, samples were preferably cut to plugs of 40 mm diameter and 30 mm length and in case of rock mechanical tests to cores of a length to diameter ratio of 2:1 at a diameter of 64 and 55 mm and the core end faces were ground parallel and perpendicular to the core axis. Tensile strength analyses were performed on disks with a height to diameter ratio of 1:2 at diameters of 64 mm and 55 mm. Although, some analyses were also performed on different sample dimensions if the method allows.

All measurements were conducted on oven-dry specimens at laboratory conditions of an average atmospheric pressure of about 0.1 MPa and at 20 °C for thermal rock properties and at approximately 23 °C for other petrophysical properties. The samples were dried in a conventional oven at 105 or 60 °C (depending on the samples clay content) until constant weight.

As follows, all applied methods are briefly described. For a more detailed methodological description please refer to Weydt et al. (2020, in review).

3.1 Thermophysical Properties

Grain (skeletal) density was determined in a gas expansion pycnometer (AccuPyc II 1340) applying helium as displacement fluid. The accuracy for grain density measurements is stated by the manufacturer as 0.02 %. Each data point is sampled from 5 single measurements. Bulk density measurements are measured with an envelope density analyzer (GeoPyc 1360). A well sorted, fine-grained powder (Dry Flo) is utilized as displacement material to determine the bulk volume of the specimen. Based on bulk volume and weight of the specimen, bulk density is calculated, which then, together with the grain density, is used for the calculation of the specimen's gas effective (or connective) porosity. The accuracy is given by the manufacturer to be within 1.1 %. Measurements comprise 3 single measurements which have been are averaged. Negative porosity values are reported on very low porous samples, but should be seen as samples with >1.1% porosity.

Dry bulk thermal conductivity and thermal diffusivity was measured using a commercial thermal conductivity scanner (Lippmann and Rauen TCS) applying the optical scanning method after Popov et al. (1999). Both parameters are measured by temperature sensors mounted on a slide moving beneath a sampling area along the core axis. For the thermal conductivity, samples and a pair of references are heated up by approximately 4°C in comparison to the ambient temperature. Thermal diffusivity is determined almost equally except that the temperature is additionally measured with a third temperature sensor shifted 7 mm perpendicular to the axis of movement. During scanning, every 1 mm a single measuring point is logged and at each logging point thermal diffusivity and conductivity is calculated based on the subsequent heating rate. The manufacturer states an accuracy within 3% of the thermal conductivity and 5% of the thermal diffusivity measurement.

Specific heat capacities are calculated after Buntebarth (1984)

$$c_p = \frac{\lambda}{\rho_{bulk} \cdot \kappa} \quad (1)$$

where c_p is the specific heat capacity, λ is the thermal conductivity, ρ_{bulk} is the bulk density and κ the thermal diffusivity.

The intrinsic permeability was measured based on the principle of Klinkenberg (1941) using a column gas permeameter, which measures the permeability of plugs applying a pressure gradient between the top and bottom surface of the sample mounted in a Hassler-cell (Filomena et al. 2014). The sample's sidewall is sealed by a rubber sleeve and an applied confining air pressure to prevent leakage. Since the intrinsic permeability reflects the effective gas permeability under infinite pressure, the intrinsic permeability is, if necessary, extrapolated based on the Klinkenberg plot of multiple single measurements of at least five different injection pressure levels at constant pressure gradients.

Apparent permeability is measured with a mini permeameter, which measures the permeability at various injection rates in the nearfield of a nozzle, pressed against the sample surface. Like the column permeameter, the mini permeameter utilizes air as measuring medium. Detection limit is 1 x 10^{-18} m² and it also needs to be addressed, that apparent permeability measurements with the mini permeameter tends to overestimate matrix permeability in low-permeable rocks.

3.2 Rock Mechanical Properties

Ultrasound wave velocities were measured using the commercial ultrasound generator Geotron USG 40 with mounted UPE-S (receiver) and UPG-S (emitter) probes, which enhance the shear wave signature. Both probes are pressed against the center of each end surface of the specimen. The contact pressure was set to 0.1 MPa and a shear gel (Magnaflux 54-T04) was applied between sample and probe to enhance the transmission of shear waves.

Dynamic elastic parameters are calculated with the equations

$$\nu_{dyn} = \frac{V_p^2 - 2V_s^2}{2(V_p^2 - V_s^2)} \quad (2)$$

$$E_{dyn} = \rho_{bulk} v_p^2 \frac{(3V_p^2 - 4V_s^2)}{(V_p^2 - V_s^2)} \quad (3)$$

where ν_{dyn} is the dynamic Poisson coefficient, E_{dyn} is the dynamic Young's modulus, ρ_{bulk} is the bulk density and V_p and V_s are the compressional and shear wave velocity.

Measurements were averaged out of 16 single measurements with a frequency of 80 kHz or 250 kHz, depending on the sample dimension and shape.

Unconfined compressive strength was tested in a 1000 kN testing frame (Form+Test Prüfsysteme) according to the ASTM D7012. Tests were both, force and displacement controlled. Strain and force rates were individually set to achieve a testing duration of approx. 10 min. Vertical displacement is measured with an external displacement transducer.

Elastic properties (Young's modulus and Poisson's ratio) are also measured in a 1000 kN test frame (Form+Test Prüfsysteme) according to the ASTM D3148 and Mutschler (2004).

Triaxial shear strength is measured in a 1000 kN test frame (Wille Geotechnik) on samples of 55 mm in diameter and 110 mm in length according to the ASTM D2664. Samples are mounted in a Hoek Cell and sealed with a rubber jacket. Confining pressures of up to 30 MPa are supplied and constantly controlled with an external pump. Hydraulic oil was chosen as confining fluid. Due to the rock strength, hard rocks were commonly measured with 5, 10 and 20 MPa confining pressure to achieve

sample failure applying the 1000 kN testing frame. The sample strain is constantly logged with an external displacement transducer, measuring the strain of the loading rod against the top platen of the testing frame. Stress and strain rates were set specifically for each sampling location to meet the given testing duration provided by the standard for each test. Cohesion and internal friction angle were determined applying the Mohr-Coulomb criterion.

Tensile (or indirect tensile) strength is determined on rock disks of 55 and 64 mm diameter at length ratios of approx. 0.5:1 (diameter to length according to ASTM D3967-16.). Therefore, the test procedure follows the Brazilian test procedure, where rock disks are compressed diametrically. Strain rates were individually set to meet the required test duration stated in ASTM D3967-16.

4 Status of the Database and Quality

To date, the database is comprised by data of either student's theses, scientific reports or self-supervised measurements conducted at the Technical University of Darmstadt. In total, 5,204 data rows (Table 3) are entered in the database which are distributed over 224 locations including quarries, abandoned quarries, outcrops and wells.

Table 3: Quantity of data entries lines categorized after the petrographic ID (rank 3, Bär et al. 2019b).

Petrographic ID	10105	10210	10322	10881	10907	69619
Petrographic Term	Plutonic Rock	Volcanic Rock	Dyke rock	Metamorphic Rock (after educt)	Metamorphic Rock (after chemistry, fabric, mineral content)	Tectonite
Data rows documented	3652	38	170	60	1216	68

As shown in Figure 3 the chosen sample locations are spread across most German outcrops of the MGCH, although many of the sampling points are concentrated in the Crystalline Odenwald. Data of the Kyffhäuser Crystalline Complex are not included in the database so far. Also, data from further wells from either the Bavarian or Rhineland-Palatinate geological services might complement the database in the future. As shown in Figure 3, more data from the Ruhla Mountains and Spessart is desirable while the Odenwald is densely sampled. Nonetheless, more complex units, such as the Flasergranitoid Zone in the northern Odenwald, should also be sampled more densely and in future, the scope should be extended to include bulk rock geochemical analysis.

Unlike databases that compile literature data of petrophysical properties (e.g. Bär et al. 2020), all data in the presented database were measured at the same institute. Therefore, the dataset is homogeneous and all data were measured under equivalent conditions and application of the same laboratory devices. Furthermore, all measurements were performed by qualified lab

professionals. Quality control was therefore an ongoing process while supervising the analyzers and reviewing the final raw and processed data, resulting in a homogeneous dataset. Quality control and reliability indices as for example presented in Bär et al. (2020) are not necessary in the presented dataset.

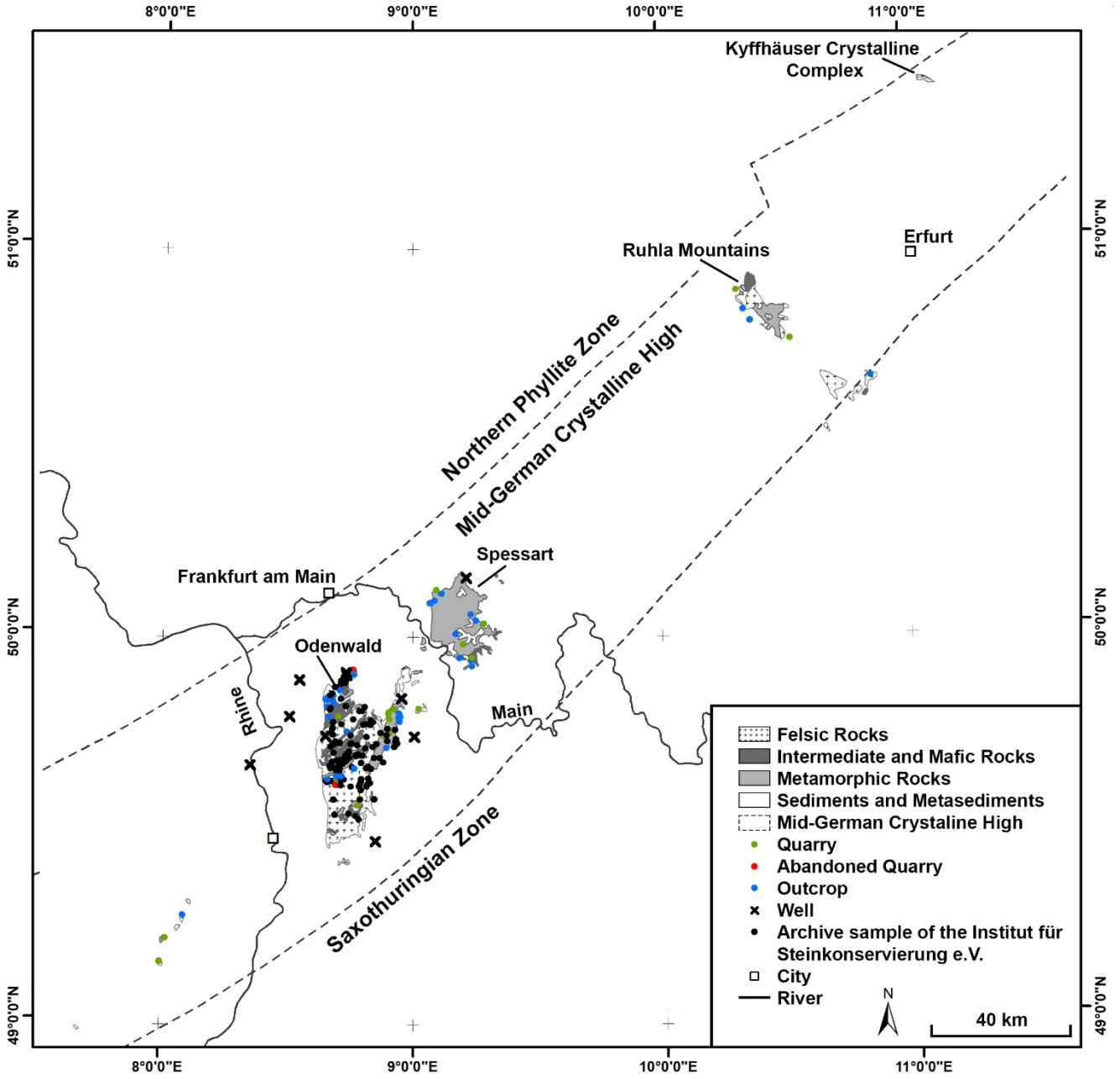

Figure 3: Sampling location of the presented database scattered around the Odenwald, Spessart and Ruhla mountains as well as well locations and outcrops in the Pfälzer Wald. Simplified overview map after (Hirschmann 1995, Voges et al. 1993, Klügel 1997, Kroner et al. 2008) of the Mid-German Crystalline High outcrops. Sampling locations from Bär (2008), Bär (2012), Biewer (2017),

Dutheillet de Lamothe (2016), Hoffmann (2015), Klaeske (2010), Lambert (2016), Maire (2014), Pei (2009), Rüther (2011), Schäffer (2012), Schäffer et al. (2018), Vogel (2016), Weber (2014), Welsch (2012) and Welsch et al. (2015).

275

4.1 Data Evaluation

Table 3 comprises minimum and maximum data of bulk density, gran density, porosity, thermal conductivity, thermal diffusivity as well as compressional and shear wave velocity of all samples reported in Weinert et al. (2020b). Besides the minimum and maximum values, an average value for each petrographic ID as well as parent ID is calculated and reported with
280 a referring standard deviation and the number of samples (n). Figure 4 displays the sample data in cross scatter plots.

Table 4: Petrophysical Properties averaged over the measured samples for each petrographic ID given in the Database Weinert et al. (2020b).

	Min	Max	Average	Standard Deviation	n
10105 – Plutonic Rock: Total Average					
Bulk Density [g cm^{-3}]	2.35	2.99	2.68	0.10	671
Grain Density [g cm^{-3}]	2.35	3.08	2.74	0.10	866
Porosity [%]	-1.43	23.79	1.89	1.97	632
Thermal Conductivity [W m^{-1} K^{-1}]	0.35	4.22	2.44	0.43	1066
Thermal Diffusivity [x10^{-6} m^2 s^{-1}]	0.53	2.63	1.22	0.26	1048
Compressional Wave Velocity [m s^{-1}]	1776	8167	4795	1116	631
Shear Wave Velocity [m s^{-1}]	1027	4811	2680	659	631
10110 – Granite					
Bulk Density [g cm^{-3}]	2.39	2.95	2.62	0.08	238
Grain Density [g cm^{-3}]	2.57	3.00	2.67	0.07	274
Porosity [%]	-1.43	9.55	1.93	1.59	233
Thermal Conductivity [W m^{-1} K^{-1}]	1.73	4.22	2.74	0.42	293
Thermal Diffusivity [x10^{-6} m^2 s^{-1}]	0.76	2.63	1.44	0.28	292
Compressional Wave Velocity [m s^{-1}]	1776	7208	4711	1116	225
Shear Wave Velocity [m s^{-1}]	1100	4038	2623	679	225

285

Continuation of Table 3: Petrophysical Properties averaged over the measured samples for each petrographic ID given in the Database Weinert et al. (2020b).

10114 – Granodiorite					
Bulk Density [g cm^{-3}]	2.42	2.87	2.69	0.07	296
Grain Density [g cm^{-3}]	2.35	2.87	2.73	0.07	378
Porosity [%]	0.01	12.27	1.82	1.88	262
Thermal Conductivity [W m^{-1} K^{-1}]	0.35	3.39	2.48	0.36	394
Thermal Diffusivity [x10^{-6} m^2 s^{-1}]	0.72	2.08	1.22	0.19	386
Compressional Wave Velocity [m s^{-1}]	1802	7046	4489	975	284
Shear Wave Velocity [m s^{-1}]	1027	3984	2541	561	284
10115 – Tonalite					
Bulk Density [g cm^{-3}]	-	-	-	-	-
Grain Density [g cm^{-3}]	-	-	-	-	-
Porosity [%]	-	-	-	-	-
Thermal Conductivity [W m^{-1} K^{-1}]	2.60	2.66	2.63	0.04	2
Thermal Diffusivity [x10^{-6} m^2 s^{-1}]	1.15	1.15	1.15	0.00	2
Compressional Wave Velocity [m s^{-1}]	-	-	-	-	-
Shear Wave Velocity [m s^{-1}]	-	-	-	-	-
10122 – Quartz Diorite					
Bulk Density [g cm^{-3}]	2.58	2.78	2.73	0.04	27
Grain Density [g cm^{-3}]	2.78	2.99	2.81	0.04	38
Porosity [%]	0.65	8	2.27	1.47	27
Thermal Conductivity [W m^{-1} K^{-1}]	1.93	2.57	2.22	0.16	38
Thermal Diffusivity [x10^{-6} m^2 s^{-1}]	0.91	1.39	1.07	0.10	38
Compressional Wave Velocity [m s^{-1}]	4172	6780	5674	642	38
Shear Wave Velocity [m s^{-1}]	1883	3979	3080	458	38

295

Continuation of Table 3: Petrophysical Properties averaged over the measured samples for each petrographic ID given in the Database Weinert et al. (2020b).

10123 – Quartz Gabbro					
Bulk Density [g cm^{-3}]	-	-	-	-	-
Grain Density [g cm^{-3}]	2.84	2.84	2.84	-	1
Porosity [%]	-	-	-	-	-
Thermal Conductivity [W m^{-1} K^{-1}]	2.35	2.35	2.35	-	1
Thermal Diffusivity [x10^{-6} m^2 s^{-1}]	1.25	1.25	1.25	-	1
Compressional Wave Velocity [m s^{-1}]	5000	5000	5000	-	1
Shear Wave Velocity [m s^{-1}]	2609	2609	2609	-	1
10131 – Diorite					
Bulk Density [g cm^{-3}]	2.35	2.89	2.72	0.10	60
Grain Density [g cm^{-3}]	2.65	3.08	2.82	0.07	111
Porosity [%]	-0.41	23.79	2.59	3.51	60
Thermal Conductivity [W m^{-1} K^{-1}]	0.95	3.81	2.13	0.37	241
Thermal Diffusivity [x10^{-6} m^2 s^{-1}]	0.53	1.73	1.05	0.17	243
Compressional Wave Velocity [m s^{-1}]	4636	8167	6122	737	51
Shear Wave Velocity [m s^{-1}]	2532	4811	3405	627	51
10132 – Gabbro					
Bulk Density [g cm^{-3}]	2.61	2.99	2.89	0.09	37
Grain Density [g cm^{-3}]	2.62	2.99	2.90	0.08	51
Porosity [%]	-0.46	4.55	0.62	0.92	37
Thermal Conductivity [W m^{-1} K^{-1}]	1.54	3.07	2.18	0.23	95
Thermal Diffusivity [x10^{-6} m^2 s^{-1}]	0.84	1.54	1.04	0.11	84
Compressional Wave Velocity [m s^{-1}]	2644	7052	5025	1283	27
Shear Wave Velocity [m s^{-1}]	1602	3886	2820	677	27

300

Continuation of Table 3: Petrophysical Properties averaged over the measured samples for each petrographic ID given in the Database Weinert et al. (2020b).

10355 – Micro Diorite					
Bulk Density [g cm^{-3}]	2.76	2.86	2.81	0.04	13
Grain Density [g cm^{-3}]	2.83	2.89	2.86	0.01	13
Porosity [%]	0.55	3.30	1.92	1.12	13
Thermal Conductivity [W m^{-1} K^{-1}]	2.38	2.44	2.41	0.04	2
Thermal Diffusivity [x10^{-6} m^2 s^{-1}]	1.35	1.39	1.37	0.03	2
Compressional Wave Velocity [m s^{-1}]	3566	5096	4409	751	5
Shear Wave Velocity [m s^{-1}]	1888	2157	1998	112	5
10210 – Volcanic Rock: Total Average					
Bulk Density [g cm^{-3}]	2.36	3.01	2.68	0.24	8
Grain Density [g cm^{-3}]	2.65	2.96	2.77	0.10	10
Porosity [%]	-0.65	13.02	5.27	5.05	8
Thermal Conductivity [W m^{-1} K^{-1}]	1.29	3.56	2.21	0.78	23
Thermal Diffusivity [x10^{-6} m^2 s^{-1}]	0.68	2.32	1.21	0.47	23
Compressional Wave Velocity [m s^{-1}]	5845	6161	6003	224	2
Shear Wave Velocity [m s^{-1}]	3219	3552	3386	236	2
10224 – Trachyte					
Bulk Density [g cm^{-3}]	-	-	-	-	-
Grain Density [g cm^{-3}]	-	-	-	-	-
Porosity [%]	-	-	-	-	-
Thermal Conductivity [W m^{-1} K^{-1}]	1.80	1.89	1.85	0.05	3
Thermal Diffusivity [x10^{-6} m^2 s^{-1}]	1.05	1.08	1.07	0.02	4
Compressional Wave Velocity [m s^{-1}]	-	-	-	-	-
Shear Wave Velocity [m s^{-1}]	-	-	-	-	-

305

Continuation of Table 3: Petrophysical Properties averaged over the measured samples for each petrographic ID given in the Database Weinert et al. (2020b).

10231 – Basalt					
Bulk Density [g cm^{-3}]	2.36	3.01	2.68	0.24	8
Grain Density [g cm^{-3}]	2.65	2.96	2.77	0.10	10
Porosity [%]	-0.65	13.02	5.27	5.05	7
Thermal Conductivity [W m^{-1} K^{-1}]	1.30	3.45	2.07	0.78	10
Thermal Diffusivity [x10^{-6} m^2 s^{-1}]	0.71	2.18	1.11	0.46	10
Compressional Wave Velocity [m s^{-1}]	5845	6161	6003	224	2
Shear Wave Velocity [m s^{-1}]	3219	3552	3386	236	2
10322 – Dyke Rock: Total Average					
Bulk Density [g cm^{-3}]	2.65	2.78	2.65	0.07	14
Grain Density [g cm^{-3}]	2.61	2.96	2.83	0.12	26
Porosity [%]	0.20	14.55	9.56	3.33	14
Thermal Conductivity [W m^{-1} K^{-1}]	1.57	3.28	2.12	0.31	47
Thermal Diffusivity [x10^{-6} m^2 s^{-1}]	0.79	1.67	1.07	0.15	49
Compressional Wave Velocity [m s^{-1}]	1120	6706	3814	1518	25
Shear Wave Velocity [m s^{-1}]	673	3341	2035	863	25
10325 – Aplite					
Bulk Density [g cm^{-3}]	2.78	2.78	2.78	-	1
Grain Density [g cm^{-3}]	2.61	2.61	2.61	-	1
Porosity [%]	0.20	0.20	0.20	-	1
Thermal Conductivity [W m^{-1} K^{-1}]	2.10	3.28	2.35	0.42	7
Thermal Diffusivity [x10^{-6} m^2 s^{-1}]	1.09	1.67	1.24	0.21	7
Compressional Wave Velocity [m s^{-1}]	-	-	-	-	-
Shear Wave Velocity [m s^{-1}]	-	-	-	-	-

Continuation of Table 3: Petrophysical Properties averaged over the measured samples for each petrographic ID given in the Database Weinert et al. (2020b).

10329 – Granitic Subvolcanic Rock					
Bulk Density [g cm^{-3}]	-	-	-	-	-
Grain Density [g cm^{-3}]	2.63	2.63	2.63	0.00	2
Porosity [%]	-	-	-	-	-
Thermal Conductivity [W m^{-1} K^{-1}]	2.56	2.61	2.58	0.03	2
Thermal Diffusivity [x10^{-6} m^2 s^{-1}]	1.32	1.34	1.33	0.01	2
Compressional Wave Velocity [m s^{-1}]	3436	3757	3596	227	2
Shear Wave Velocity [m s^{-1}]	2012	2069	2041	40	2
10336 – Porphyric Granite					
Bulk Density [g cm^{-3}]	2.53	2.74	2.64	0.05	13
Grain Density [g cm^{-3}]	2.90	2.96	2.94	0.02	13
Porosity [%]	6.71	14.55	10.28	2.04	13
Thermal Conductivity [W m^{-1} K^{-1}]	1.57	1.98	1.81	0.11	13
Thermal Diffusivity [x10^{-6} m^2 s^{-1}]	0.82	1.05	0.94	0.07	13
Compressional Wave Velocity [m s^{-1}]	1120	3271	1600	656	13
Shear Wave Velocity [m s^{-1}]	673	1874	1300	298	13
10337 – Porphyric Granodiorite					
Bulk Density [g cm^{-3}]	-	-	-	-	-
Grain Density [g cm^{-3}]	2.68	2.70	2.69	0.01	4
Porosity [%]	-	-	-	-	-
Thermal Conductivity [W m^{-1} K^{-1}]	2.38	2.48	2.44	0.04	4
Thermal Diffusivity [x10^{-6} m^2 s^{-1}]	1.12	1.24	1.18	0.05	4
Compressional Wave Velocity [m s^{-1}]	4993	5809	5399	466	4
Shear Wave Velocity [m s^{-1}]	3021	3341	3192	150	4

Continuation of Table 3: Petrophysical Properties averaged over the measured samples for each petrographic ID given in the Database Weinert et al. (2020b).

10360 – Porphyric Diorite					
Bulk Density [g cm^{-3}]	-	-	-	-	-
Grain Density [g cm^{-3}]	2.74	2.78	2.76	0.02	3
Porosity [%]	-	-	-	-	-
Thermal Conductivity [W m^{-1} K^{-1}]	2.05	2.56	2.18	0.17	9
Thermal Diffusivity [x10^{-6} m^2 s^{-1}]	0.92	1.19	1.04	0.11	9
Compressional Wave Velocity [m s^{-1}]	4297	5622	4857	686	3
Shear Wave Velocity [m s^{-1}]	2624	3310	2893	366	3
58823 – Diabase					
Bulk Density [g cm^{-3}]	-	-	-	-	-
Grain Density [g cm^{-3}]	-	-	-	-	-
Porosity [%]	-	-	-	-	-
Thermal Conductivity [W m^{-1} K^{-1}]	1.70	2.04	1.88	0.14	4
Thermal Diffusivity [x10^{-6} m^2 s^{-1}]	0.79	1.09	1.02	0.12	6
Compressional Wave Velocity [m s^{-1}]	-	-	-	-	-
Shear Wave Velocity [m s^{-1}]	-	-	-	-	-
58827 – Dioritic Lamprophyre					
Bulk Density [g cm^{-3}]	-	-	-	-	-
Grain Density [g cm^{-3}]	-	-	-	-	-
Porosity [%]	-	-	-	-	-
Thermal Conductivity [W m^{-1} K^{-1}]	2.49	2.49	2.49	-	1
Thermal Diffusivity [x10^{-6} m^2 s^{-1}]	1.12	1.12	1.12		1
Compressional Wave Velocity [m s^{-1}]	-	-	-	-	-
Shear Wave Velocity [m s^{-1}]	-	-	-	-	-

Continuation of Table 3: Petrophysical Properties averaged over the measured samples for each petrographic ID given in the Database Weinert et al. (2020b).

58830 – Kersantite					
Bulk Density [g cm^{-3}]	-	-	-	-	-
Grain Density [g cm^{-3}]	2.82	2.83	2.83	0.01	3
Porosity [%]	-	-	-	-	-
Thermal Conductivity [W m^{-1} K^{-1}]	2.01	2.36	2.17	0.15	7
Thermal Diffusivity [x10^{-6} m^2 s^{-1}]	0.95	1.11	1.05	0.07	7
Compressional Wave Velocity [m s^{-1}]	5431	6707	6061	638	3
Shear Wave Velocity [m s^{-1}]	2634	3017	2815	192	3
10907 – Metamorphic Rock (Total)					
Bulk Density [g cm^{-3}]	2.33	3.05	2.68	0.12	281
Grain Density [g cm^{-3}]	2.50	3.12	2.71	0.12	336
Porosity [%]	-0.57	10.35	1.36	1.56	265
Thermal Conductivity [W m^{-1} K^{-1}]	1.24	6.00	2.61	0.54	988
Thermal Diffusivity [x10^{-6} m^2 s^{-1}]	0.52	5.80	1.35	0.39	902
Compressional Wave Velocity [m s^{-1}]	1553	7456	4589	1069	256
Shear Wave Velocity [m s^{-1}]	1103	3890	2550	584	256
10895 – Meta Granite					
Bulk Density [g cm^{-3}]	-	-	-	-	-
Grain Density [g cm^{-3}]	2.62	2.70	2.67	0.03	9
Porosity [%]	-	-	-	-	-
Thermal Conductivity [W m^{-1} K^{-1}]	2.44	3.22	2.81	0.19	43
Thermal Diffusivity [x10^{-6} m^2 s^{-1}]	1.11	1.95	1.51	0.23	43
Compressional Wave Velocity [m s^{-1}]	1093	6570	4765	825	25
Shear Wave Velocity [m s^{-1}]	1912	3436	2809	403	25

Continuation of Table 3: Petrophysical Properties averaged over the measured samples for each petrographic ID given in the Database Weinert et al. (2020b).

10898 – Meta Gabbro					
Bulk Density [g cm^{-3}]	-	-	-	-	-
Grain Density [g cm^{-3}]	-	-	2.88	-	1
Porosity [%]	-	-	-	-	-
Thermal Conductivity [W m^{-1} K^{-1}]	2.39	2.67	2.51	0.14	3
Thermal Diffusivity [x10^{-6} m^2 s^{-1}]	0.95	1.11	1.05	0.09	3
Compressional Wave Velocity [m s^{-1}]	5202	5789	5496	415	2
Shear Wave Velocity [m s^{-1}]	3111	3262	3186	106	2
10917 – Quartzite					
Bulk Density [g cm^{-3}]	2.62	2.62	2.62	0.00	2
Grain Density [g cm^{-3}]	2.65	2.65	2.65	0.00	2
Porosity [%]	1.16	1.16	1.16	0.00	2
Thermal Conductivity [W m^{-1} K^{-1}]	5.24	6.11	5.73	0.44	3
Thermal Diffusivity [x10^{-6} m^2 s^{-1}]	3.67	4.18	3.96	0.26	3
Compressional Wave Velocity [m s^{-1}]	-	-	-	-	-
Shear Wave Velocity [m s^{-1}]	-	-	-	-	-
10926 – Phyllite					
Bulk Density [g cm^{-3}]	-	-	-	-	-
Grain Density [g cm^{-3}]	-	-	-	-	-
Porosity [%]	-	-	-	-	-
Thermal Conductivity [W m^{-1} K^{-1}]	2.45	4.14	3.37	0.45	11
Thermal Diffusivity [x10^{-6} m^2 s^{-1}]	-	-	-	-	-
Compressional Wave Velocity [m s^{-1}]	-	-	-	-	-
Shear Wave Velocity [m s^{-1}]	-	-	-	-	-

335

Continuation of Table 3: Petrophysical Properties averaged over the measured samples for each petrographic ID given in the Database Weinert et al. (2020b).

10945 – Gneiss					
Bulk Density [g cm^{-3}]	2.33	2.82	2.62	0.05	186
Grain Density [g cm^{-3}]	2.55	2.88	2.65	0.04	199
Porosity [%]	0.01	10.35	1.14	1.27	178
Thermal Conductivity [W m^{-1} K^{-1}]	1.60	3.53	2.79	0.32	198
Thermal Diffusivity [x10^{-6} m^2 s^{-1}]	0.60	1.98	1.36	0.20	194
Compressional Wave Velocity [m s^{-1}]	1886	6150	4291	1062	131
Shear Wave Velocity [m s^{-1}]	1103	3489	2334	551	131
10949 – Biotite Gneiss					
Bulk Density [g cm^{-3}]	2.62	2.75	2.65	0.04	11
Grain Density [g cm^{-3}]	2.51	2.77	2.63	0.08	13
Porosity [%]	0.06	4.46	1.62	1.58	9
Thermal Conductivity [W m^{-1} K^{-1}]	1.96	2.98	2.46	0.27	34
Thermal Diffusivity [x10^{-6} m^2 s^{-1}]	0.88	1.67	1.39	0.19	30
Compressional Wave Velocity [m s^{-1}]	-	-	-	-	-
Shear Wave Velocity [m s^{-1}]	-	-	-	-	-
10961 – Garnet Biotite Gneiss					
Bulk Density [g cm^{-3}]	2.73	2.74	2.74	0.00	3
Grain Density [g cm^{-3}]	2.74	2.76	2.75	0.01	5
Porosity [%]	0.15	0.50	0.33	0.25	2
Thermal Conductivity [W m^{-1} K^{-1}]	2.57	4.15	3.63	0.43	18
Thermal Diffusivity [x10^{-6} m^2 s^{-1}]	0.71	1.94	1.64	0.29	18
Compressional Wave Velocity [m s^{-1}]	-	-	-	-	-
Shear Wave Velocity [m s^{-1}]	-	-	-	-	-

340

Continuation of Table 3: Petrophysical Properties averaged over the measured samples for each petrographic ID given in the Database Weinert et al. (2020b).

10966 – Garnet Plagioclase Gneiss					
Bulk Density [g cm^{-3}]	-	-	-	-	-
Grain Density [g cm^{-3}]	-	-	-	-	-
Porosity [%]	-	-	-	-	-
Thermal Conductivity [W m^{-1} K^{-1}]	4.21	4.21	4.21	-	1
Thermal Diffusivity [x10^{-6} m^2 s^{-1}]	2.34	2.34	2.34	-	1
Compressional Wave Velocity [m s^{-1}]	-	-	-	-	-
Shear Wave Velocity [m s^{-1}]	-	-	-	-	-
10968 – Hornblende Biotite Gneiss					
Bulk Density [g cm^{-3}]	2.63	2.95	2.76	0.06	15
Grain Density [g cm^{-3}]	2.69	2.94	2.77	0.05	29
Porosity [%]	0.00	2.18	0.45	0.58	12
Thermal Conductivity [W m^{-1} K^{-1}]	1.75	4.46	2.55	0.62	30
Thermal Diffusivity [x10^{-6} m^2 s^{-1}]	0.94	2.76	1.35	0.48	25
Compressional Wave Velocity [m s^{-1}]	-	-	-	-	-
Shear Wave Velocity [m s^{-1}]	-	-	-	-	-
10970 – Muscovite Biotite Gneiss					
Bulk Density [g cm^{-3}]	2.61	2.64	2.63	0.01	6
Grain Density [g cm^{-3}]	2.50	2.61	2.57	0.05	6
Porosity [%]	0.33	5.35	2.70	2.11	5
Thermal Conductivity [W m^{-1} K^{-1}]	1.92	2.62	2.36	0.23	18
Thermal Diffusivity [x10^{-6} m^2 s^{-1}]	0.94	1.89	1.53	0.27	18
Compressional Wave Velocity [m s^{-1}]	-	-	-	-	-
Shear Wave Velocity [m s^{-1}]	-	-	-	-	-

Continuation of Table 3: Petrophysical Properties averaged over the measured samples for each petrographic ID given in the Database Weinert et al. (2020b).

10989 – Amphibolite					
Bulk Density [g cm^{-3}]	2.33	3.05	2.85	0.14	56
Grain Density [g cm^{-3}]	2.60	3.12	2.90	0.12	66
Porosity [%]	-0.57	10.35	2.16	2.14	55
Thermal Conductivity [W m^{-1} K^{-1}]	1.24	3.80	2.20	0.40	80
Thermal Diffusivity [x10^{-6} m^2 s^{-1}]	0.63	2.40	1.09	0.24	80
Compressional Wave Velocity [m s^{-1}]	1896	6305	4931	1000	19
Shear Wave Velocity [m s^{-1}]	1173	3520	2806	547	19
10990 – Biotite-bearing Amphibolite					
Bulk Density [g cm^{-3}]	2.58	2.63	2.61	0.04	2
Grain Density [g cm^{-3}]	2.64	2.66	2.65	0.02	2
Porosity [%]	1.11	2.15	1.63	0.73	2
Thermal Conductivity [W m^{-1} K^{-1}]	2.33	2.56	2.48	0.13	3
Thermal Diffusivity [x10^{-6} m^2 s^{-1}]	1.52	1.57	1.54	0.03	3
Compressional Wave Velocity [m s^{-1}]	-	-	-	-	-
Shear Wave Velocity [m s^{-1}]	-	-	-	-	-
10543 – Schist					
Bulk Density [g cm^{-3}]	-	-	-	-	-
Grain Density [g cm^{-3}]	-	-	-	-	-
Porosity [%]	-	-	-	-	-
Thermal Conductivity [W m^{-1} K^{-1}]	2.00	2.03	2.01	0.02	2
Thermal Diffusivity [x10^{-6} m^2 s^{-1}]	1.00	1.00	1.00	0.00	2
Compressional Wave Velocity [m s^{-1}]	-	-	-	-	-
Shear Wave Velocity [m s^{-1}]	-	-	-	-	-

355 **Continuation of Table 3: Petrophysical Properties averaged over the measured samples for each petrographic ID given in the Database Weinert et al. (2020b).**

69620 – Cataclastite					
Bulk Density [g cm^{-3}]	-	-	-	-	-
Grain Density [g cm^{-3}]	2.62	2.68	2.65	0.02	4
Porosity [%]	-	-	-	-	-
Thermal Conductivity [W m^{-1} K^{-1}]	2.65	3.39	3.00	0.26	13
Thermal Diffusivity [x10^{-6} m^2 s^{-1}]	1.27	1.77	1.52	0.19	13
Compressional Wave Velocity [m s^{-1}]	3746	5576	4540	917	4
Shear Wave Velocity [m s^{-1}]	1896	3388	2673	703	4

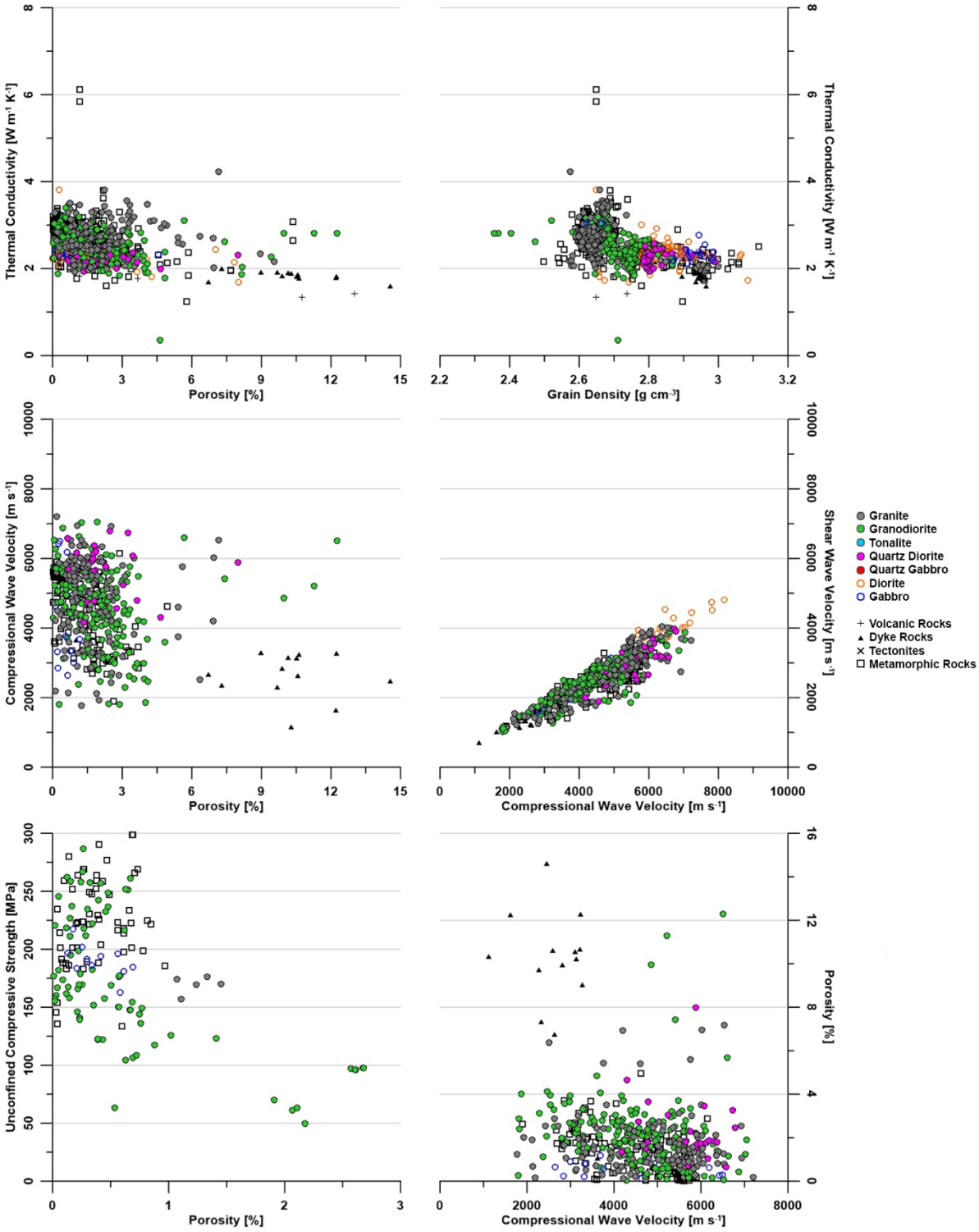

Figure 4: Scatter plots of the most common petrophysical properties of the data set of Weinert et al. (2020b).

5 Data Availability

The complete dataset of thermophysical and rock mechanical properties can be accessed at https://doi.org/10.25534/tudatalib-278 (Weinert et al., 2020b).

6 Discussion

The compilation of comprehensive databases always requires critical review of the input data. Often, published data do not match the minimum requirements of the dataset (as e.g. mentioned in Bär et al., 2020). All data stored in the presented database were measured at the same institution applying the same methods. Therefore, all data presented conform to the same standards and quality requirements. This also ensures a high comparability of the measurements since the methodological accuracy and errors are identical throughout the dataset. Due to the coherence of the presented dataset, the documented properties are easy to correlate and can help to understand petrophysical properties within the Mid-German Crystalline High but also allows deriving general correlations between petrophysical properties itself (e.g. Figure 4).

The described correlations and data ranges are also in good agreement with previous studies of rock of the Mid-German Crystalline High (e.g. Kushnir et al. 2018) but also crystalline basement rocks of various different locations (e.g. Carmichael,1989 and references therein; Mielke et al., 2017; Kushnir et al. 2018) such as e.g. the Gonghe Basin Complex (Weinert et al. 2020a). The correlations of porosity against thermal conductivity but also compressional wave velocity are in accordance with findings of Mielke et al. (2017). Decreasing compressional wave velocities with increasing porosities is in accordance with findings of e.g. Kushnir et al. (2018) or Weinert et al. (2020a). The same negative correlation is found for porosity and unconfined compressive strength (e.g. the presented data set; Li and Aubertin, 2003 Kushnir et al. (2018); Weinert et al., 2020a).

Advantageous to many other databases are the metadata attached to each measurement and specimen. Therefore, petrophysical properties can easily be extracted and applied in other studies or for parametrization of local to regional numerical models. Nonetheless, the presented data may need to be individually processed (e.g. upscaled) to fit application such as large-scaled geothermal modelling. Such data processing can be required since the presented data only represent laboratory-scale matrix properties. Such small-scaled data may vary significantly in larger rock masses. Such scale effects are most prominently observed on matrix and bulk permeabilities. Matrix permeabilities (or permeabilities measured in the laboratory) commonly underestimate the bulk reservoir permeability (as data of e.g. Stober and Jodocy, 2009 or Vidal and Genter, 2018 suggest) due to neglecting permeability of any fractures or fracture network. Datasets such as provided by Achtziger-Zupančič et al. (2017) and Scibek (2020) can provide valuable information for reservoir scale permeability estimations also in nearfields of fault zones. Manning and Ingebritsen (1999), Ingebritsen and Manning (2010) and Stober and Bucher (2015) published data on reservoir scale permeabilities of the upper crust which can be used for assessing and upscaling matrix permeabilities as provided in the presented database. In general, a variety of different upscaling methods are developed, applied, and reviewed (e.g. Wen and Gómez-Hernández 1996; Farmer 2002; Qi and Hesketh, 2005). Techniques can be as simple as applying power

law averages on a representative elementary volume (e.g. Qi and Hesketh 2005) but can also require the integration of a fracture network model (e.g. Bao et al., 2012). Since the published methods for upscaling petrophysical properties are plenty, a close consideration of the applied processes is necessary. The method always needs to be chosen regarding the researched application, rock type or geological setting.

8 Sample Availability

Most of the samples are available at the Technical University of Darmstadt and are stored for at least 10 years after finalization of a student's thesis or scientific report. Data that are labelled with 'archive samples of the Institut für Steinkonservierung' (column 'Outcrop Type') were sampled in their archive and it may be possible to request the samples directly at the Institut für Steinkonservierung e. V. In case of well samples, please refer to the Hessian Agency for Nature Conservation, Environment and Geology. For samples of the wells Weiterstadt 1, Worms 3 and Stockstadt 33R please refer to the Bundesverband Erdgas, Erdöl und Geoenergie e. V.

9 Acknowledgement

The authors thank Dr. Karin Kraus from the the Institut für Steinkonservierung e. V. for providing their archive samples for analyzation. Further, the authors are thankful to the Bundesverband Erdgas, Erdöl und Geoenergie e. V. (BVEG) as well as BEB Erdgas und Erdöl GmbG & Co. KG, the owner of the wells, for providing core samples of the crystalline basement for investigation and publishing. The authors also thank the Hessian Agency for Nature Conservation, Environment and Geology (HLNUG), especially Dr. Johann-Gerhard Fritsche as well as Dr. Gerald Gabriel from the Leibniz Institute for Applied Geophysics (LIAG) and Dr. Sonja Wedmann from the Senkenberg Research Institute and Natural History Museum for providing access to the well cores.

As research assistants Alexander Lambert, Christian Schneider and Stina Krombach helped in measuring the presented data. The authors are further thankful for the help of Florent Dutheillet de Lamothe within the framework of his internship at Technical University of Darmstadt. Also, the authors are grateful for contributions of Bianca Vogel, Alexander Lambert, Rafael Schäffer, Helmuth Hoffmann, Romain Maire, Alexej Philipp, Johanna Rüther, Jan Niklas Weger, Ulrike Klaeske, Liang Pei, and Hendrik Biewer in the framework of their conducted student theses.

Furthermore, the authors thank for the financial support by the DFG in the framework of the Excellence Initiative, Darmstadt Graduate School of Excellence Energy Science and Engineering (GSC 1070) as well as the Federal Ministry for Economic Affairs and Energy for financing the present research in the scope of Hessen 3D 2.0 (funding number 0325944A)

References

Achtziger-Zupančič, P., Loew, S., Mariéthoz, G.: A new global database to improve predictions of permeability distribution in crystalline rocks at site scale. Journal of Geophysical Research: Solid Earth, https:doi.org/10.1002/2017JB014106, 2017

Aretz, A., Bär, K., Götz, A. E., Sass, I.: Outcrop analogue study of Permocarboniferous geothermal sandstone reservoir formations (northern Upper Rhine Graben, Germany): impact of mineral content, depositional environment and diagenesis on petrophysical properties, International Journal of Earth Sciences105(5), https://doi.org/10.s00531-015-1263-2, 2016.

Anthes, G., Reischmann, T.: Timing of granitoid magmatism in the eastern mid-German crystalline rise. Journal of Geodynamics, 31(2), https://doi.org/10.1016/S0264-3707(00)00024-7, 2001

ASTM International. D3148 Standard test method for elastic moduli of intact rock core specimens in uniaxial compression, West Conshohocken, PA; ASTM International. https://doi.org/10.1520/D3148-02, 2002.

ASTM International: D2664-04 Standard test method for triaxial compressive strength of undrained rock core specimens without pore pressure measurements, West Conshohocken, PA; ASTM International. https://doi.org/10.1520/D2664-04, 2004.

ASTM International: D7012-14e1 Standard test methods for compressive strength and elastic moduli of intact rock core specimens under varying states of stress and temperatures. West Conshohocken, PA; ASTM International. https://doi.org/10.1520/D7012-14E01, 2014.

ASTM International: D3967-16 Standard test method for splitting tensile strength of intact rock core specimens, West Conshohocken, PA; ASTM International. https://doi.org/10.1520/D3967-16, 2016.

Bao, K., Salama, A., Sun, S.: Upscaling of permeability field of fractured rock systems: Numerical examples. Journal of Applied Mathematics, https://doi.org/10.1155/2012/546203, 2012.

Bär, K. M.: 3D-Modellierung des tiefengeothermischen Potenzials des nördlichen Oberrheingrabens und Untersuchung der geothermischen Eigenschaften des Rotliegend. Diploma Thesis, Technical University of Darmstadt (in German with English abstract), 2008

Bär, K. M.: Untersuchung der tiefengeothermischen Potenziale von Hessen. PhD Thesis, Technical University of Darmstadt (in German with English abstract). Available at: https://tuprints.ulb.tu-darmstadt.de/3067/, 2012.

Bär, K. and Mielke, P.: Stratigraphic classification table (Stratigraphy): P³ - Stratigraphy. V. 1.0. GFZ Data Services. Potsdam. http://dx.doi.org/10.5880/GFZ.4.8.2019.P3.s, 2019a.

Bär, K., Mielke, P. and Knorz, K.: Petrographic classification table (Petrography): P³ - Petrography. V. 1.0. GFZ Data Services. Potsdam. http://dx.doi.org/10.5880/GFZ.4.8.2019.P3.p, 2019b.

Bär, K., Reinsch, T., Bott, J.: P³ - PetroPhysicalProperty Database – a global compilation of lab measured rock properties, Earth System Science Data, https://doi.org/10.5194/essd-2020-15, 2020.

Biewer, H.: Vergleich von Eigenschaften petrothermaler Reservoirgesteine des Gonghe-Beckens und Tromm-Granits/Weschnitz-Plutons. Master Thesis, Technical University of Darmstadt (in German with English abstract), 2017.

Brätz, H.: Radiometrische Altersdatierung und geochemische Untersuchung von Orthogneisen, Graniten und Granitporphyren aus dem Ruhlaer Kristallin, Mitteldeutsche Kristallinzone, PhD Thesis, Bayerische Julius-Maximilians-Universität Würzburg (in German), 2000.

Buntebart, G.: Geothermics – An introduction, Springer-Verlag Berlin Heidelberg, 1984.

Carmicheal, R. S.: Practical Handbook of physical properties of rocks and minerals. CRC Press, Boca Raton, 1989.

Cohen, K. M., Finney, S. C., Gibbard, R. L., Fan, J.-X.: The ICS International Chronistratigraphic Chart, episodes, 36: 199-204, 2013, updated.

Deutscher Bundestag: Drucksache 15/1835,15, Wahlperiode 24.10.2003, Bericht des Ausschusses für Bildung, Forschung und Technikfolgenabschätzung (17. Ausschuss) gemäß §56a der Geschäftsordnung. Technikfolgenabschätzung: Monitoring – Möglichkeiten geothermischer Stromerzeugung in Deutschland (in German), 2003

Dombrowsky, A., Henjes-Kunst, F., Höhndorf, A., Kröner, A., Okrusch, M., Richter, O.: Orthogneisses in the Spessart Crystalline Complex, Northwest Bavaria: Witnesses of Silurian granitoids magmatism at an active continental margin, Geologische Rundschau, 84, 1995.

Dutheillet de Lamothe, F.: Petrophysical characterization or rocks and correlation of these properties with geochemical and mineralogical composition. Internship Report, Technical University of Darmstadt, 2016.

Farmer, C. L.: Upscaling: a review. International Journal for Numerical Methods in Fluids, https://doi.org/10.1002/fld.267, 2002.

Filomena, C. M., Hornung, J., stollhofen, H.: Assessing accuracy of gas-driven permeability measurements: a comparative study of diverse Hassler-cell and probe permeameter devices. Solid Earth, 5, 2014.

Hirschmann, G.: Lithological characteristics (Mid-German Crystalline Rise). In Dallmeyer, R. D., Franke, F., Weber, K (eds): Pre-Permian geology of Central and Eastern Europe. Springer Verlag, Berlin, 155-163, 1995.

Hoffmann, H.: Petrophysikalische Eigenschaften der Mitteldeutschen Kristallinschwelle im Bereich des Oberrheingrabens. Master Thesis, Technical University of Darmstadt (in German with English abstract), 2015.

Howell, J.A., Martinius, A.W., Good, T.R.: The application of outcrop analogues in geological modelling: a review, present status and future outlook. In: Martinius, A. W., Howell, J. A. & Good, T. R. (eds) 2014. Sediment-Body geometry and heterogeneity: Analogue studies for modelling the subsurface, Geological Society, London, Special Publications, 387, 1–25. https://doi.org/10.1144/SP387.12, 2014

Ingebritsen, S. E., Manning, C. E.: Permeability of the continental crust: dynamic variations inferred from seismicity and metamorphism. Geofluids, 10, 193-205, https://doi.org/ 10.1111/j.1468-8123.2010.00278.x, 2010.

Kirsch, H., Kober, B., Lippolt, H. J.: Age of intrusion and rapid cooling of the Frankenstein gabbro (Odenwald, SW-Germany) evidence by $^{40}Ar/^{39}Ar$ and single zircon $^{207}Pb/^{206}Pb$ measurements, Geologische Rundschau, 77, 1988.

Klaeske, U.: Bestimmung des geothermischen Potenzials des Kristallinen Odenwaldes. Bachelor Thesis, Technical University of Darmstadt (in German with English abstract), 2010.

Klinkenberg, L. J.: The permeability of porous media to liquids and gases. Drilling Production Practice, API, 1941.

Klügel, T., Geometrie und Kinematrik einer variszischen Plattengrenze. Der Südrand des Rhenoherzynikums im Taunus, Geologische Abhandlungen Hessen, 101 (in German), 1997.

Krietsch, H., Doetsch, J., Dutler, N., Jalali, M., Gischig, V., Loew, S., Amann, F.: Comprehensive geological dataset describing a crystalline rock mass for hydraulic stimulation experiments. Nature Scientific Data, https://doi.org/10.1038/sdata.2018.269, 2018.

Kroner, U., Mansy, J.-L. Mazur, S., Aleksandrowsky, P., Hann, H. P., Huckriede, H., Lacquement, F., Lamarche, J., Ledru, P., Pharaoh, T. C., Zedler, H., Zeh, A., Zulauf, G.: Variscan tectonic. In: McCann, T. (ed) 2008. The geology of Central Europe. Volume 1: Precambrian and Palaeozoic. Geological Society, London, 599-664, 2008.

Lambert, A.-D.: Bestimmung der petrophysikalischen und felsmechanischen Kennwerte des Tromm- und Weschnitz-Plutons, Odenwald, Deutschland. Bachelor Thesis, Technical University of Darmstadt (in German with English abstract), 2016.

Li, L, Aubertin, M.: A general relationship between porosity and uniaxial strength of engineering materials. Canadian Journal of Civil Engineering, 30, 644-658, https://doi.org/10.1139/l03-012, 2003

Linnemann, U., Romer, R. L., Pin, C., Aleksandrowsky, P., Bula, Z., Geisler, T., Kachlik, V., Krzeminska, E., Mazur, S., Motuza, G., Murphy, J. B., Nance, R. D., Pisarevsky, S. A., Schulz, B., Ulrich, J., Wiszniewska, J., Zaba, J., Zeh, A.: Precambrian. In: McCann, T. (ed) 2008. The geology of Central Europe. Volume 1: Precambrian and Palaeozoic. Geological Society, London, 21-102, 2008.

Lippolt, H. J.: Nachweis altpaläozoischer Primäralter (Rb-Sr) und karbonischer Abkühlalter (K-Ar) der Muskovit-Biotit-Gneise des Spessarts und der Biotit-Gneise des Böllsteiner Odenwaldes, Geologische Rundschau, 75 (in German), 1986.

Machek, M., Roxerová, Z., Janoušek, V., Staněk, M., Petrovský, E. René, M.: Petrophysical and geochemical constraints on alteration processes in granites. Studia Geophysica et Geodaetica 57, https://doi.org/10.1007/s11200-013-0923-6, 2013

Maire, R.: Investigation of thermo-physical and mechanical parameters of crystalline geothermal reservoir rocks of the Upper Rhine Graben (Germany). Master Thesis, LaSalle Beauvais, Technical University of Darmstadt, 2014.

Manning, C. E., Ingebritsen, S. E.: Permeability of the continental crust: implications of geothermal data and metamorphic systems. Reviews of Geophyiscs, 37, 127-150, https://doi.org/10.1029/1998RG900002, 1999

McCann, T.: The geology of Central Europe. Volume 1: Precambrian and Palaeozoic. Geological Society, London, 2008.

Mielke, P., Weinert, S., Bignall, G., Sass, I.: Thermo-physical rock properties of greywacke basement rock and intrusive lavas from the Taupo Volcanic Zone, New Zealand. Journal of Volcanology and Geothermal Research, 324, 2016.

Mutschler, T.: Neufassung der Empfehlung Nr.1 des Arbeitskreises Versuchstechnik Fels der Deutschen Gesellschaft für Geotechnik e. V.: Einaxiale Druckversuche an zylindrischen Gesteinsprüfkörpern. Bautechnik, 81, 2004.

Okrusch, M.: The Spessart crystalline complex, Northwest Bavaria. DMG SFMC Joint Meeting 1983, Excursion E4, Fortschritte der Mineralogie, 61 (in German), 1983.

Pei, L.: Analysis of initiation and propagation of hydraulically induced fracture. Master Thesis, Technical University of Darmstadt, 2009.

Popov, Y. A., Pribnow, D. F. C., Sass, J. H., Williams, C. F., Burkhardt, H.: Characterization of rock thermal conductivity by high resolution optical scanning. Geothermics, 28(2), 1999.

Qi, D., Hesketh, T.: An analysis of upscaling techniques for reservoir simulation. Petroleum Science and Technology 23(7-9), 827-842, https://doi.org/10.1081/LFT-200033132, 2005.

Reischmann, T., Anthes, G., Jaeckel, P., Altenberger, U.: Age and origin oft he Böllsteiner Odenwald, Mineralogy and Petrology, 72, 2001.

Rüther, J.: Thermofazielle Interpretation des Permokarbons im Sprendlinger Horst. Diploma Thesis, Technical University of Darmstadt (in German with English abstract), 2011.

Sass, I., Weinert, S., Bär, K.: Success rates of petroleum and geothermal wells and their impact on the European geothermal industry. – Swiss Bull. Angew. Geol. 21(2), 54-65, https://doi.org/10.5169/seals-658197, 2016.

Schäffer, R.: Hydrogeologische und geothermische Untersuchungen der Heilquellen und Heilbrunnen Bad Soden-Salmünsters. Diploma Thesis, Technical University of Darmstadt (in German with English abstract), 2012.

Schäffer, R., Bär, K. and Sass, I.: Multimethod exploration of the hydrothermal reservoir in Baden Soden-Salmünster, Germany. Zeitschrift der Deutschen Gesellschaft für Geowissenschaften (German Journal of Geology), 169(3). https://doi.org/10.1127/zdgg/2018/0147, 2018.

Scibek, J.: Multidisciplinary database of permeability of fault zones and surrounding protolith rocks at world-wide sites. Scientific Data, 7, 95, https://doi.org/10.1038/s41597-020-0435-5, 2020.

Stein, E.: The geology of the Odenwald Crystalline Complex. Mineralogy and Petrology, 72, 2001.

Stober, I., Bucher, K.: Hydraulic conductivity of fractured upper crust: insights from hydraulic tests in boreholes and fluid-rock interaction in crystalline basement rocks. Geofluids, 15, 161-178, https://doi.org/10.1111/gfl.12104, 2015.

Stober, I., Jodocy, M: Eigenschaften geothermischer Nutzhorizonte im baden-württembergischen und französischen Teil des Oberrheingrabens, Grundwasser, 14, https://doi.org/10.1007/s00767-009-0103-3, 2008.

Timmerman, M. J.: Palaezoic magmatism. In: McCann, T. (ed) 2008. The geology of Central Europe. Volume 1: Precambrian and Palaeozoic. Geological Society, London, 665-748, 2008.

Todt, W. A., Altenberger, U., Raumer, J. F.: U-Pb data on zicrons for the thermal peak of metamorphism in the Variscan Odenwald, Germany, Geologische Rundschau, 84 (in German), 1995.

Ukar, E., Laubach, S.E., Hooker, J. N.: Outcrops as guides to subsurface natural fractures: Example from the Nikanassin Formation tight-gas sandstone, Grande Cache, Alberta foothills, Canada. Marine and Petroleum Geology 103. 255–275. https://doi.org/10.1016/j.marpetgeo.2019.01.039, 2019.

Vidal, J., Genter, A.: Overview of naturally permeable fractured reservoirs in the central and southern Upper Rhine Graben: Insights from geothermal wells. Geothermics, 74. 57-73 https://doi.org/10.1016/j.geothermics.2018.02.003, 2018.

Vogel, B. C.: Petrophysikalische und felsmechanische Untersuchung kristalliner Gesteine des Weschnitz-Plutons. Bachelor Thesis, Technical University of Darmstadt (in German with English abstract), 2016.

Voges, A., Toloczyki, M., Trurnit, P. Wittekindt, H.: Geologiesche Karte der Bundesrepublik Deutschland 1:1.000.000. BGR, Hannover, 1993.

Weber, J. N.: Geothermische Aufschlussanalyse des Steinbruches Mainzer Berg, östlich von Darmstadt. Bachelor Thesis, Technical University of Darmstadt (in German with English abstract), 2014.

Weinert, S., Bär, K., Sass, I.: Thermophysical rock properties of the crystalline Gonghe Basin Complex (Northeastern Qinghai–Tibet-Plateau, China) basement rocks. Environmental Earth Sciences, 79, 2020a.

Weinert, S., Bär, K., Sass, I.: Petrophysical Properties of the Mid-German Crystalline High: A Database for Bavarian, Hessian, Rhineland-Palatinate and Thuringian Outcrops. TUdatalib, https://doi.org/10.25534/tudatalib-278, 2020b.

Welsch, B.: Forschungsbohrung Heubach: Untersuchungen zu den geothermischen Reservoireigenschaften des Odenwald Kristallins. Diploma Thesis, Technical University of Darmstadt (in German with English abstract), 2012.

Welsch, B., Baer, K., Schulte, D., Rühaak, W., Chauhan, S.: Simulation und Evaluierung von Kopplungs- und Speicherkonzepten regenerativer Energieformen zur Heizwärmeversorgung. Final report, Technical University of Darmstadt (in German with English abstract), 2015.

Wen, X-h., Gómez-Hernández, J.J.: Upscaling hydraulic conductivities in heterogeneous media: An overview. Journal of Hydrogeology, https://doi.org/10.1016/S0022-1694(96)80030-8, 1996.

Weydt, L., Ramírez-Guzmán, Á. A., Pola A., Lepillier, B., Kummerow, J., Mandrone, G., Comina, C., Deb, P., Norini, G., Gonzalez-Partida, E., Avellán, D. R., Marcías, J. L., Bär, K., Sass, I.: Petrophysical and mechanical rock property database of the Los Humeros and Acoculco geothermal fields (Mexico). Earth System Science Data (PrePrint), 2020.

Will, T., M., Schmädicke, E.: A first report of eclogites in the Odenwald Crystalline Complex: evidence for high-pressure metamorphism in the Mid-German Crystalline Rise, Germany. Lithos, 59, 2001.

Zeh, A., Wunderlich, J.: Mitteldeutsche Kristallinzone. In: Seidel, G. (ed) 2003: Geologie von Thüringen. E. Schweitzbart'sche Verlagsbuchhandlung, Stuttgart, 24-51, 2003.

Zeh, A., Williams, I. S., Brätz,H., Millar, I. L.: Different age response of zircon and monazite during the tectonometamorphic evolution of a high grade paragneiss from the Ruhla Crystalline Complex, Central Germany. Contributions to Mineralogy and Petrology, 145, 2003.